nanomaterials

MDPI

Article

Monolayer AsC_5 as the Promising Hydrogen Storage Material for Clean Energy Applications

Qiang Lu, Binyuan Zhang, Lianlian Zhang, Yulian Zhu and Weijiang Gong *

College of Sciences, Northeastern University, Shenyang 110819, China
* Correspondence: gwj@mail.neu.edu.cn

Abstract: One of the critical techniques for developing hydrogen storage applications is the advanced research to build novel two-dimensional materials with significant capacity and effective reversibility. In this work, we perform first-principles unbiased structure search simulations to find a novel AsC_5 monolayer with a variety of functionally advantageous characteristics. Based on theoretical simulations, the proposed AsC_5 has been found to be energetically, dynamically, and thermally stable, supporting the viability of experiment. Since the coupling between H_2 molecules and the AsC_5 monolayer is quite weak due to physisorption, it is crucial to be enhanced by thoughtful material design. Hydrogen storage capacity can be greatly enhanced by decorating the AsC_5 monolayer with Li atoms. Each Li atom on the AsC_5 substrate is shown to be capable of adsorbing up to four H_2 molecules with an advantageous average adsorption energy (E_{ad}) of 0.19 eV/H_2. The gravimetric density for hydrogen storage adsorption with 16Li and 64 H_2 of a Li-decorated AsC_5 monolayer is about 9.7 wt%, which is helpful for the possible application in hydrogen storage. It is discovered that the desorption temperature (T_D) is much greater than the hydrogen critical point. Therefore, such crucial characteristics make AsC_5-Li be a promising candidate for the experimental setup of hydrogen storage.

Keywords: AsC_5 monolayer; hydrogen storage material; first-principles calculations

Citation: Lu, Q.; Zhang, B.; Zhang, L.; Zhu, Y.; Gong, W. Monolayer AsC_5 as the Promising Hydrogen Storage Material for Clean Energy Applications. *Nanomaterials* **2023**, *13*, 1553. https://doi.org/10.3390/nano13091553

Academic Editor: Diego Cazorla-Amorós

Received: 14 March 2023
Revised: 10 April 2023
Accepted: 13 April 2023
Published: 5 May 2023

1. Introduction

As fossil fuel consumption increases and reserves decrease, it is imminent to develop new energy sources in today's world [1,2]. Hydrogen energy is exactly this kind of secondary energy source that is green and low-carbon, widely used, and rich in sources [3–5]. The main links of the hydrogen energy industry chain include the preparation, storage, transportation, and utilization of hydrogen [6,7]. The hydrogen storage in the middle of the industry chain connects the production of hydrogen and the application of hydrogen. It is the key technology and prerequisite for the large-scale application of hydrogen. Realization of safe and effective hydrogen storage is the decisive factor for restricting the large-scale application of hydrogen energy [8–10]. The current technology for storing hydrogen in liquid and gaseous forms have restrictions in terms of weight, size, safety, and cost. A potential remedy for this issue, however, is the reversible storage of hydrogen in solid form [11–16]. The following two crucial considerations should be taken into account when selecting the hydrogen storage technique. The average adsorption energy (E_{ad}) of adsorbed hydrogen on the possible adsorptive medium (−0.1 to −0.6 eV) is the first crucial factor [17]. The second is a gravimetric hydrogen storage capability that meets the U.S. Department of Energy's (DOE) 2020 objective of 5.5 wt% [18]. Currently, we are unaware of any hydrogen storage materials that fulfill this stringent requirement. Hence, there is a critical need to develop a novel high-capacity material for storing hydrogen.

Among the various available options, carbonous materials possess a great potential for H_2 storage applications due to their large specific surface area, light weight, and numerous adsorption sites. After the successful exfoliation of graphene, the enthusiasm for developing

inorganic carbon-based materials has grown to a great extent [19–21]. Due to their excellent electrical, optical, thermal, and mechanical properties, carbon-based materials are widely used [22,23]. Not only do they play an important role in nanoelectronic devices, but they also play a vital role in clean energy such as solar cells and hydrogen storage [24–26]. For instance, Ghanbari et al. investigated graphene's potential application as a hydrogen storage material and found that graphene doped with Si and/or Ge has a large hydrogen molecule storage capacity [27]. Labrousse revealed that the volumetric and gravimetric capabilities of GeC_3 may reach up to 98.41 g/dm^3 and 7.25 wt%, respectively, [28]. Research into the storage of H_2 in two-dimensional (2D) materials has shown that metal defects and decoration improve storage capacity relative to pure materials [29–31]. For example, H_2 had only a limited interaction with pure MoS_2 (adsorption energy of just −0.023 eV), but it was robustly adsorbed on the Ti-decorated MoS_2 (−0.472 eV) [32]. At the same time, along with transition metals and alkali earth metals, alkali metal atoms are considered to be the preferred object because a large number of studies have confirmed that they play an important role in effectively improving hydrogen storage density due to their small cohesive energy and light atomic weight [33–35]. Lithium, as the alkali metal at the top of the periodic table, is preferred because of its light atomic weight and highest hydrogen storage weight ratio. For example, Li-doped graphene [36], CN monolayer [37], and B_2S monolayer [38] all show excellent hydrogen storage performance.

This research is inspired by the aforementioned reasons; thus, given that C materials have outstanding conduction and stability qualities, our main focus is on AsC_5 compositions rich in C. We conduct a thorough structural search to identify the monolayer that is the most stable [39]. As anticipated, we observe a novel AsC_5 monolayer with a graphene-like buckling structure (see Figure 1). Following that, phonon calculations and AIMD simulations are used to examine the structural stability. Then, density functional theory (DFT) simulations are used to examine the viability of the Li-decorated AsC_5 film as a hydrogen storage material. We confirm that the hydrogen binding energy is enhanced by Li decoration on the AsC_5 monolayer. Moreover, it is found that in the fully loaded case, the hydrogen storage density is up to 9.7 wt%, which is in excellent agreement with the standards set by the US Department of Energy. Additionally, the desorption temperature (T_D) of this system ranges from 243 to 357 K, significantly greater than hydrogen's critical temperature (33 K). In this regard, AsC_5-based materials are considered to be candidates for excellent hydrogen storage of clean energy applications.

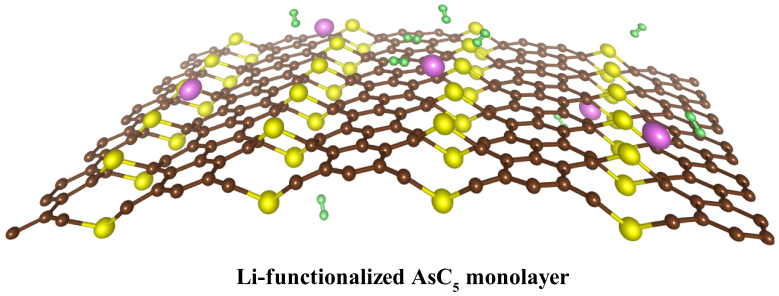

Figure 1. Schematic diagram of hydrogen storage on Li-functionalized AsC_5. The green dots denote the H atoms, yellow dots describe the As atoms, brown dots correspond to C atoms, and purple dots are the Li atoms.

2. Method

To identify the lowest energy structures of AsC_5 monolayers, the particle swarm optimization (PSO) approach is used inside the evolutionary process as implemented in the CALYPSO package [39,40]. A total of 60% of the structures from the first generation with lower Gibbs free energies are chosen for PSO construction of the structures of the following generation. In the next generation, 40% of the structures are produced at random. The variety of the structures is greatly increased by these processes, which is critical for the

efficiency of a structural global search. Significantly, theoretical computations are crucial for both finding novel 2D materials and comprehending the underlying physical processes behind observed experimental findings [41–44].

The Vienna ab initio Simulation Package (VASP) is employed for our first-principles computations [45,46]. In this code, the Kohn–Sham equations are solved within a pseudopotential approximation, in which the popular generalized gradient approximation (GGA) of the PBE function is utilized to describe the exchange-correlation energy and potential between electrons [47]. Furthermore, van der Waals corrections have been included using the DFT-D3 method of Grimme to model the interaction at the interface [48,49]. For the structural relaxation, the total energy tolerances and maximum atomic forces are within 1.0×10^{-6} eV and 0.01 eV/Å, respectively. The isolation of slab models are created with a vacuum of 20 Å to avoid unphysical interactions between periodically repeated images. A mesh of $8 \times 4 \times 1$ k for the unit cell and $4 \times 2 \times 1$ k for the 2×2 supercell system are used [50] for the integration of the Brillouin zone, and the kinetic energy cutoff is set to 500 eV. The ab initio Molecular Dynamic Simulation (AIMD) is utilized to predict thermal stability, and a Nose–Hoover thermostat framework is used for temperature regulation [51].

3. Results and Discussion

According to the PSO technique and DFT calculations, we design a novel AsC_5 monolayer, as shown in Figure 2a. One can find that ten C and two As atoms construct the AsC_5 monolayer in the rectangle-shaped unity cell, and the AsC_5 monolayer displays the buckled structure. Next, relaxed lattice constants and monolayer thicknesses of AsC_5 are found to be $a = 4.41$ Å, $b = 8.08$ Å, and 1.83 Å. The C-C and As-C bond lengths are calculated as 1.42 Å and 1.98 Å, respectively. Furthermore, Figure 2b clearly shows the electronic band structure and projected density of states (PDOS) of AsC_5. It is shown that the AsC_5 monolayer exhibits a similar Dirac cone with a tiny band gap (0.01 eV). From the PDOS, we observe that the p-orbits of C atoms contribute mostly to the conduction band minimum and valence band maximum of the AsC_5 monolayer.

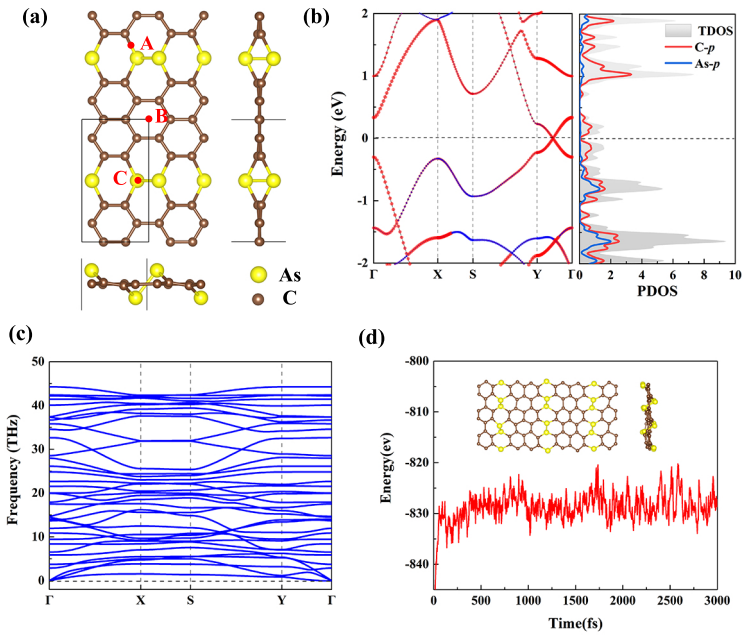

Figure 2. (**a**) Optimized crystal structures of the AsC_5 monolayer (Top and side views). (**b**) The electronic band structure and PDOS spectra of the AsC_5 monolayer. (**c**) Phonon dispersion curves of AsC_5 monolayer. (**d**) AIMD plots at 1000 K for 3 ps of AsC_5. The inset shows that the structure of AsC_5 after dynamics simulations.

The structural stability of any material is critical for its practical application; thus, we estimate the phonon dispersion curve to prove dynamical stability of AsC_5. From Figure 2c, one can see that no negative frequencies are identified in any of the acoustic branches which branch out from Γ. This strongly suggests that the AsC_5 monolayer is dynamically stable. In addition, the thermodynamic stability of AsC_5 monolayer is confirmed by employing AIMD simulations, and we find no significant reorganization of structure and bonds broken after the relaxation of 3 ps at 1000 K with energies fluctuating slightly (see Figure 2d). Finally, the cohesive energy of AsC_5 is calculated to explore the mechanical strength. According to the research results, the AsC_5 monolayer has the cohesive energy of 6.72 eV/atom, which is higher than that of arsenene (2.95 eV/atom) [52] and almost as high as that of graphene (7.98 eV/atom) [53]. Based on the above data, we expect that the AsC_5 monolayer can be synthesized experimentally.

To evaluate the hydrogen storage capability of pristine AsC_5 nanosheets, we adopt a $2 \times 2 \times 1$ supercell and put one H_2 molecule on various potential locations to comprehensively investigate H_2 adsorption capability on the AsC_5 monolayer. As shown in Figure 2a, three potential adsorption sites are selected depending on the symmetry of AsC_5, including the bridge site (A) of the C-As bond, the hollow site (B) above the C-C ring, and the top site (C) on the As atom. The average adsorption energy (E_{ad}) is calculated by the following expression:

$$E_{ad} = (E_{AsC_5+nH_2} - E_{AsC_5} - nE_{H_2})/n, \quad (1)$$

where $E_{AsC_5+nH_2}$ is the energy of the AsC_5 monolayer after adsorption of n H_2 molecules and E_{AsC_5} is the energy of the pristine AsC_5 monolayer. E_{H_2} represents the energy of single H_2 molecule. The calculated E_{ad} of a H_2 molecule at A-site, B-site, and C-site is -0.037 eV, -0.043 eV, and -0.020 eV per H_2, respectively (Table 1). The vertical adsorption distances of H_2 to AsC_5 are 2.30 Å, 1.71 Å, and 2.52 Å, respectively. This is caused by the buckling structure of the AsC_5 material. As C-site is close to the protruding As atom, it receives strong repulsion, so the vertical adsorption distance is larger and the corresponding adsorption energy is reduced. Adsorbed H_2 is found to have a H-H bond length (l) of 0.75 Å, which is equal to the free H_2, indicating that the adsorbed H_2 is unaffected by AsC_5. Furthermore, it is discovered that the minimal H_2 adsorption energy occurs at the B-site (see Figure 3a), and its adsorption energy, which is far below -0.1 eV, is insufficient to store hydrogen. The electrons in the s shell of the H_2 and the p shells of carbon are hybridized, with the energy close to -6.0 eV, according to the comparison of the PDOS depicted in Figures 2b and 3b.

Table 1. The calculated adsorption energy (E_{ad}), the adsorption height (h), H-H bond length (l) of hydrogen molecule, and the calculated binding energy (E_b) of a single Li-decorated AsC_5 system and Bader charge analysis of a Li atom at A, B, and C-sites.

	E_{ad} (eV)	h (Å)	l (Å)	E_b (eV)	Q
A	−0.037	2.30	0.75	−2.33	0.57
B	−0.043	1.71	0.75	−2.36	0.77
C	−0.020	2.52	0.75	−2.34	0.63

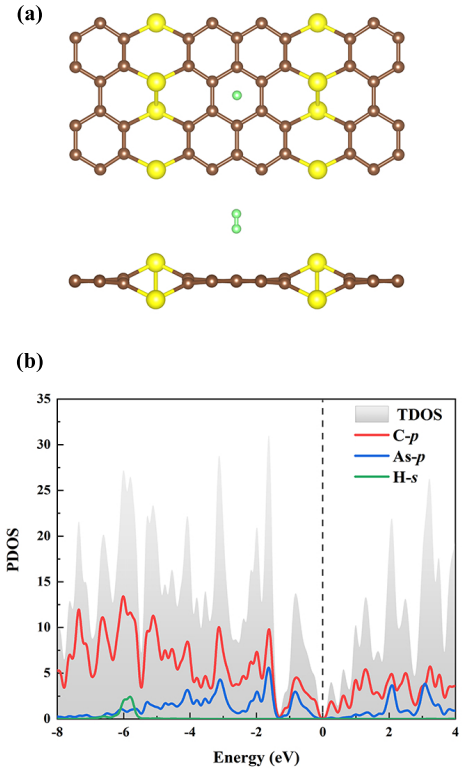

Figure 3. (**a**) Optimization diagram of the adsorption of H_2 on the AsC_5 monolayer. (**b**) PDOS of single H_2 adsorbed on pure AsC_5 at the B adsorption site.

In order to study the effect of Li modification on the hydrogen storage capacity of AsC_5, we start by putting a single Li atom at each of the adsorption sites depicted in Figure 2a. The decorated Li atom's binding energy (E_b) to the AsC_5 is given by the equation below:

$$E_b = (E_{AsC_5-mLi} - E_{AsC_5} - mE_{Li})/m, \quad (2)$$

where E_{AsC_5-mLi}, E_{Li}, and m represent the total energy of the AsC_5 compound with m doped Li atoms, the energy of a free Li atom, and the number of Li atoms adsorbed, respectively. Table 1 summarizes the binding energy characteristics of Li and the corresponding charge transfer at the position considered on the surface of AsC_5. The findings reveal that the Li atoms have a preference for being adsorbed above the center site of the hexagonal honeycomb (B site), with an E_b of −2.36 eV (see Figure 4a for the optimized structure). The decorating of the Li atom on the AsC_5 is an exothermic process since the E_b value is negative. Additionally, it is important to note that the absolute value of the E_b of the Li atom's adsorption on B-site is larger than the cohesive energy of Li bulk (1.61 eV). This demonstrates the potential dispersion and stability of Li atom on the AsC_5 [54].

Next, we investigate the charge density difference between Li-adsorbed AsC_5 and pristine AsC_5 to explore the electrochemical contact between Li and AsC_5 with Equation (2):

$$\Delta\rho = \rho_{AsC_5-Li} - \rho_{AsC_5} - \rho_{Li}. \quad (3)$$

ρ_{Li}, ρ_{AsC_5}, and ρ_{AsC_5-Li} are the charge densities of an isolated Li, pristine AsC_5, and adsorption systems, respectively. Figure 4b shows an obvious charge redistribution in the interface area, where charge accumulation is primarily on the AsC_5 surface and depletion is near the Li atoms. This suggests that Li ions bond strongly to the AsC_5 monolayer as a consequence of electrons being transported from Li to the substrate. Additionally, the precise quantity of the charge transfer is determined by Bader charge analysis (see Table 1). In the stable adsorption sites, around 0.57–0.77 e is transported from Li to AsC_5 sheet, indicative of an

ionic interaction between Li and AsC_5. To understand the conductivity of sodiated AsC_5, the PDOS is calculated and shown in Figure 4c. It is worth noting that when Li is adsorbed on the AsC_5 monolayer, the system exhibits metallicity due to a slight downward shift of the conduction band compared with the pristine AsC_5.

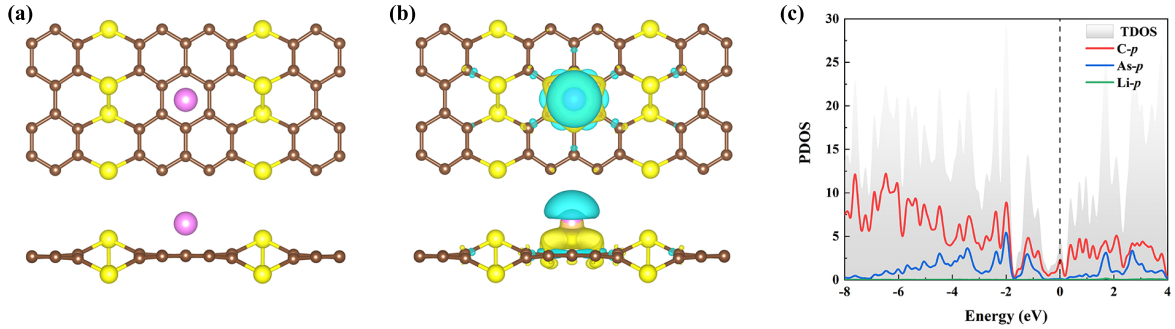

Figure 4. (**a**) Optimized structure and (**b**) charge density differences of Li-decorated AsC_5 on the B-site. The isosurface is set to 0.002 e/Bohr^3. (**c**) The corresponding PDOS of the AsC_5 monolayer decorated with one Li atom.

After assessing the viability of Li decoration on the AsC_5 monolayer, further investigation into the hydrogen storage capability of this system can be performed. The consecutive adsorption energy (E_{ca}) of H_2 molecules can be calculated as follows:

$$E_{ca} = E_{AsC_5-Li+(n-1)H_2} + E_{H_2} - E_{AsC_5-Li+(n)H_2}. \quad (4)$$

In this formula, n stands for the number of H_2 molecules, and $E_{AsC_5-Li+(n-1)H_2}$ and $E_{AsC_5-Li+(n)H_2}$ are the total energies of nH_2 molecules and $(n-1)H_2$ absorbed on the AsC_5 monolayer of the decorated system by Li, respectively. It can be seen from Figure 5 that the adsorption of hydrogen steadily rises from left to right. The substrate AsC_5-Li shows slight deformation following hydrogen adsorption, indicating that the adsorbent has excellent cycle performance. The results show that the first H_2 molecule is adsorbed on the AsC_5-Li compound with an adsorption energy of -0.31 eV/H_2 and the bond length of H-H is 0.76 Å (Table 2). It should be noticed that the E_{ad} of H_2 on AsC_5-Li is nearly eight times greater than that on the pure AsC_5 monolayer. As more H_2 molecules are introduced to the compound, the E_{ad} value of the molecules decreases until it reaches -0.24 eV/H_2 for the AsC_5-Li compound. The adsorption energy, which is suggested to be in the region of -0.1 to -0.6 eV, is obviously perfect for hydrogen storage.

Table 2. Calculated average Li-H_2 distance (d), the average H-H bond lengths (l), the average adsorption (E_{ad}), and the consecutive adsorption (E_{ca}) energies of H_2 molecules.

n	d (Å)	l (Å)	E_{ad}	E_{ca}
1	2.04	0.76	−0.31	0.31
2	2.07	0.76	−0.29	0.29
3	2.49	0.76	−0.28	0.24
4	2.43	0.76	−0.27	0.23
5	2.70	0.75	−0.24	0.12

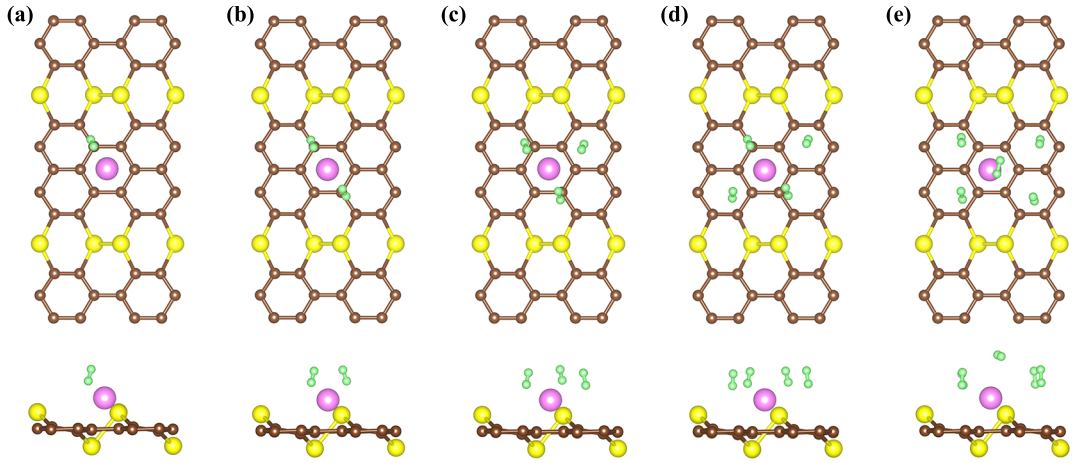

Figure 5. The optimized structures of 1–5 (**a**–**e**) H_2 adsorbed on AsC_5-Li.

At the same time, electron localization function (ELF) is investigated to further study the interaction between H_2 and pure AsC_5 or Li-modified AsC_5, as shown in Figure 6. The blue areas indicate that the ELF value between H_2 and pure AsC_5 is very close to zero (see Figure 6a), meaning that no electrons are shared in this adsorbed system and no new bonds are formed. This is strong evidence that H_2 can only physically adsorb to the pure AsC_5 monolayer, since no ELF region of chemical bonding has been observed. On the other hand, a significant electron localization overlap is detected between adsorbed H_2 and AsC_5-Li, as shown in Figure 6b. One can find the electron sharing in the AsC_5-Li mode and the chemical properties of H_2 adsorption by Li-decorated AsC_5. Next, Figure 6c shows that the prominent peak of H-s around 9 eV is overlapped strongly with the Li-p, the C-p, and As-p. This illustrates the strong hybridization between the adsorbed H_2 and the decorated Li atom in the modified AsC_5. Additionally, the PDOS analysis combined with the total electron density and ELF results confirms the strong adsorption of H_2 on AsC_5-Li.

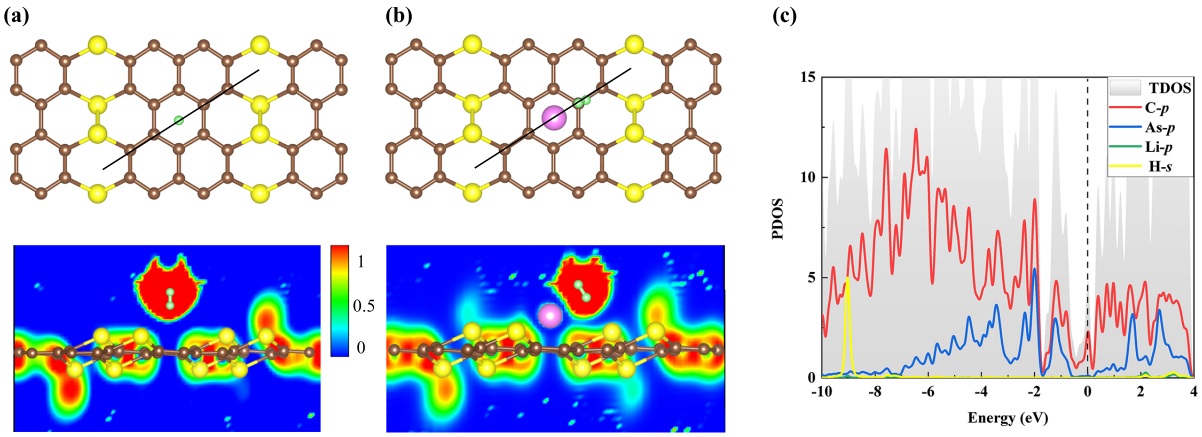

Figure 6. ELF profiles of the adsorption of one H_2 on (**a**) the pure AsC_5 or (**b**) the Li-decorated one. (**c**) The corresponding PDOS spectra.

The possibility of adding more Li atoms to each side of the AsC_5 monolayer is also taken into account. The calculated average E_b of 4, 8, and 16 Li atoms decorated on the AsC_5 monolayer are −0.44, −0.41, and −0.36 eV/Li, respectively. To confirm the stability of AsC_5-xLi, we perform the AIMD simulation of AsC_5-16Li at 1000 K for 3 ps. As shown in Figure 7a, AsC_5-16Li could keep its structural integrity without significant alterations. Furthermore, in the AIMD simulation, there is a tiny variation in energy. All of the findings suggest that AsC_5-16Li is thermally stable at 1000 K. As can be seen in Figure 7b, we also

carry out an analysis of the PDOS results. They confirm the strong bond between the AsC_5 monolayer and Li atom by demonstrating an evident hybridization between the p-orbits of the C and As atoms and the p-orbits of the Li atoms. Moreover, as mentioned above, AsC_5 has a tiny band gap (0.01 eV) and presents semi-metallic properties, indicating good conductivity, which has a positive influence on Li embedding/desorption.

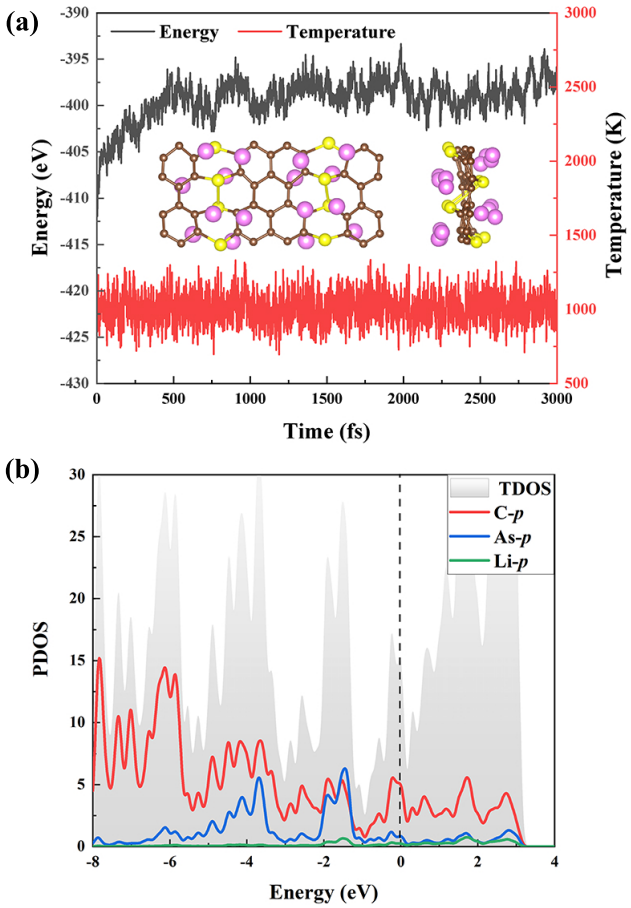

Figure 7. (**a**) Energy and temperature fluctuations during AIMD simulation. Inset: the configurations after 3 ps at 1000 K. (**b**) The PDOS spectra of AsC_5-16Li.

Regarding practical H_2 storage applications, reversible H_2 adsorption/liberation at room temperature is crucial. The temperature of desorption (T_D) typically increases with increasing adsorption energy for H_2 molecules. T_D for H_2 molecules with different adsorption numbers at AsC_5-16Li has been calculated in the current investigation using the equation below [55]:

$$T_D(K) = (\frac{|E_b|}{K_B})(\frac{\Delta S}{R} - \ln P)^{-1}. \quad (5)$$

K_B, R, and ΔS are, respectively, the Boltzmann constant, gas constant (8.31 J/mol K), and change in the H_2 molecule's entropy (S) from gas to liquid phase at the balance pressure (i.e., the 1 atm). The gravimetric density of H_2 storage is calculated by employing the formula

$$C_g = \frac{M_{H_2}}{M_{H_2} + M_{host}}, \quad (6)$$

where M_{H_2} and M_{host} denote the total weight of the adsorbed H_2 and the Li-decorated AsC_5, respectively. For the decorated systems (AsC_5-16Li), we discover that the T_D values lie in the range of 243–357 K (see Figure 8a), which are significantly larger than most other

2D materials such as Be_2C-Li/K (163/129 K), BP-Li/Na (116/95 K), and GeC_3 (224 K). We also note that the T_D of the AsC_5-16Li substrate is significantly greater (>7 times) than the hydrogen critical temperature.

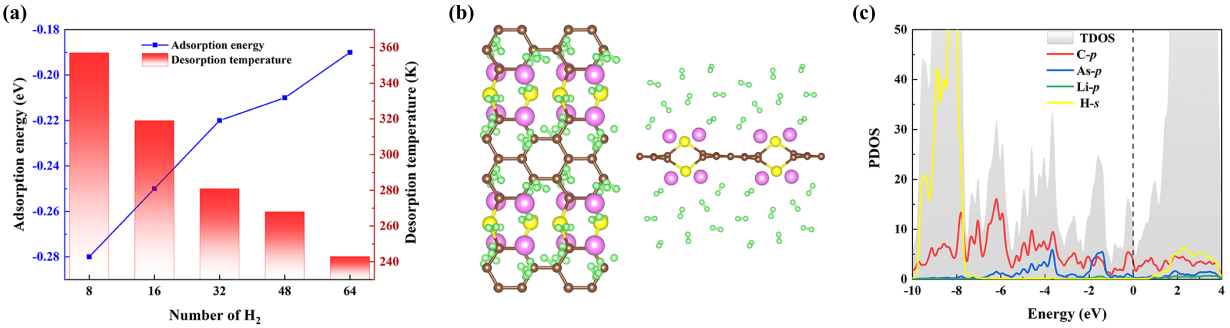

Figure 8. (**a**) Average adsorption energies and desorption temperature as a function of the number of adsorbed hydrogen molecules on AsC_5-16Li. (**b**) The optimized systems of maximum hydrogen molecules adsorption on AsC_5-16Li. (**c**) PDOS of 64 H_2 adsorbed on AsC_5-16Li.

As shown in Figure 8b, on the AsC_5-16Li substance, a maximum of 4 H_2 molecules can be adsorbed on each Li with an energy of −0.19 eV/H_2, so the gravimetric density of hydrogen storage of this system is enhanced to 9.7 wt%. A comparison of the s-orbit of H and p-orbit of Li in the PDOS is given in Figure 8c, and the results demonstrate no clear hybridization, implying their weak interaction with each other. It is known that the hydrogen storage of carbon-based materials has been the subject of numerous prior research. The results in Table 3 show that the hydrogen density varies greatly for different materials, depending on the choice of the doped metal atoms and substrate. Note also that the hydrogen storage capacity found in our research is greater than that of the majority of the materials mentioned. Furthermore, by taking into account the outstanding thermodynamically stable conditions, which is another crucial criterion for hydrogen storage materials, one can ascertain that Li-decorated AsC_5 is a viable candidate for the application of the hydrogen storage material.

Table 3. Hydrogen density of different materials.

Structure	wt%
B@r57-Li4	10
Li-decorated T4,4,4-graphyne	10.46
Ti-decorated MoS_2	5.93
Pd-decorated Si_2BN	6
Ti-decorated graphene	7.8
GeC_3	7.25
Li-decorated Be_2C	10.21
Li-decorated AsC_5 (This work)	9.7

4. Summary

To summarize, in this work we have employed the first-principles DFT computations to establish and calculate the pristine and Li-decorated AsC_5 sheets. As a result, it has been found that Li atoms on the surface of the AsC_5 monolayer could be adjusted in a stable manner with their negative adsorption energy. The hydrogen molecule has a modest interaction with unmodified AsC_5, but a strong interaction with AsC_5 that is decorated with a single Li atom. H_2 adsorbed on the modified AsC_5 has an adsorption energy of −0.31 eV, which is nearly 7 times greater than that of the pristine AsC_5 (−0.04 eV). Overall, up to 64 H_2 molecules could be adsorbed on both sides of AsC_5-16Li, and the average energy is well within the ideal range for desorption temperature and effective hydrogen storage properties. The maximal gravimetric hydrogen storage capacity of Li-decorated AsC_5 can

reach 9.7 wt%, which is greater than that of the majority of carbon-based materials. All of these appealing properties indicate that the Li-doped AsC_5-based material has great potential as a reversible hydrogen storage material that can be used as clean alternative fuel for transportation.

Author Contributions: Q.L.: Investigation. B.Z.: Software, Validation. L.Z.: Writing—original draft. Y.Z.: Software, Validation. W.G.: Writing—review & editing. All authors have read and agreed to the published version of the manuscript.

Funding: This work was funded by the LiaoNing Revitalization Talents Program (Grant No. XLYC1907033), the National Natural Science Foundation of China (Grant No. 11905027), and the Fundamental Research Funds for the Central Universities of Ministry of Education of China (Grant Nos. N2205015 and N2002005).

Institutional Review Board Statement: Not applicable.

Informed Consent Statement: Not applicable.

Data Availability Statement: Data available on request from the authors.

Conflicts of Interest: The authors declare no conflict of interest.

References

1. Jacobson, M.Z. Review of solutions to global warming, air pollution, and energy security. *Energy Environ. Sci.* **2009**, *2*, 148–173. [CrossRef]
2. Qu, Y.; Duan, X. Progress, challenge and perspective of heterogeneous photocatalysts. *Chem. Soc. Rev.* **2013**, *42*, 2568–2580. [CrossRef]
3. Konda, R.; Deshmukh, A.; Kalamse, V.; Chaudhari, A. Functionalized tetrahedral silsesquioxane cages for hydrogen storage. *Int. J. Hydrogen Energy* **2020**, *45*, 32157–32167. [CrossRef]
4. Sherif, S.A.; Barbir, F.; Veziroglu, T.N. Wind energy and the hydrogen economy—Review of the technology. *Sol. Energy* **2005**, *78*, 647–660. [CrossRef]
5. Jacobson, M.Z.; Colella, W.G.; Golden, D.M. Cleaning the air and improving health with hydrogen fuel cell vehicles. *Science* **2005**, *308*, 1901–1905. [CrossRef] [PubMed]
6. Kittner, N.; Lill, F.; Kammen, D.M. Energy storage deployment and innovation for the clean energy transition. *Nat. Energy* **2017**, *2*, 17125. [CrossRef]
7. Cheng, H.M.; Yang, Q.H.; Liu, C. Hydrogen storage in carbon nanotubes. *Carbon* **2001**, *39*, 1447–1454. [CrossRef]
8. Glenk, G.; Reichelstein, S. Economics of converting renewable power to hydrogen. *Nat. Energy* **2019**, *4*, 216–222. [CrossRef]
9. Hirscher, M.; Yartys, V.A.; Baricco, M.; Colbe, J.M.B.V.; Blanchard, D.; Bowman, R.C.; Broom, D.P.; Buckley, C.E.; Chang, F.; Chen, P. Materials for hydrogen-based energy storage-past, recent progress and future outlook. *J. Alloys Compd.* **2020**, *827*, 153548. [CrossRef]
10. Midilli, A.; Ay, M.; Dincer, I.; Rosen, M.A. On hydrogen and hydrogen energy strategies I: Current status and needs. *Renew. Sust. Energy Rev.* **2005**, *9*, 255–271. [CrossRef]
11. Dillon, A.C.; Jones, K.M.; Bekkedahl, T.A.; Kiang, C.H.; Bethune, D.S.; Heben, M.J. Storage of hydrogen in single-walled carbon nanotubes. *Nature* **1997**, *386*, 377. [CrossRef]
12. Sathe, R.Y.; Bae, H.; Lee, H.; Kumar, T.J.D. Hydrogen storage capacity of low-lying isomer of C24 functionalized with Ti. *Int. J. Hydrogen Energy* **2020**, *45*, 9936–9945. [CrossRef]
13. Liu, Z.; Hussain, T.; Karton, A.; Er, S. Empowering hydrogen storage properties of haeckelite monolayers via metal atom functionalization. *Appl. Surf. Sci.* **2021**, *556*, 149709. [CrossRef]
14. Panigrahi, P.; Desai, M.; Talari, M.K.; Bae, H.; Lee, H.; Ahuja, R. Selective decoration of nitrogenated holey graphene (C_2N) with titanium clusters for enhanced hydrogen storage application. *Int. J. Hydrogen Energy* **2021**, *46*, 7371–7380. [CrossRef]
15. Mou, Z.; Dong, Y.; Li, S.; Du, Y.; Wang, X.; Yang, P.; Wang, S. Eosin Y functionalized graphene for photocatalytic hydrogen production from water. *Int. J. Hydrogen Energy* **2011**, *36*, 8885–8893. [CrossRef]
16. Zheng, S.; Fang, F.; Zhou, G.; Chen, G.; Ouyang, L.; Zhu, M.; Sun, D. Hydrogen storage properties of space-confined $NaAlH_4$ nanoparticles in ordered mesoporous silica. *Chem. Mater.* **2008**, *20*, 3954–3958. [CrossRef]
17. Jin, X.; Qi, P.; Yang, H.; Zhang, Y.; Li, J.; Chen, H. Enhanced hydrogen adsorption on Li-coated $B_{12}C_6N_6$. *J. Chem. Phys.* **2016**, *145*, 164301. [CrossRef]
18. Zhang, X.; Tang, C.; Jiang, Q. Electric field induced enhancement of hydrogen storage capacity for Li atom decorated graphene with Stone-Wales defects. *Int. J. Hydrogen Energy* **2016**, *41*, 10776–10785. [CrossRef]
19. Novoselov, K.S.; Geim, A.K.; Morozov, S.V.; Jiang, D.; Zhang, Y. Electric field effect in atomically thin carbon films. *Science* **2004**, *306*, 666–669. [CrossRef]

20. Yu, L.; Pan, X.; Cao, X.; Hu, P.; Bao, X. Oxygen reduction reaction mechanism on nitrogen-doped graphene: A density functional theory study. *J. Catal.* **2011**, *282*, 183–190. [CrossRef]
21. Dai, C.L.; Sun, G.Q.; Hu, L.Y.; Xiao, Y.K.; Zhang, Z.P.; Qu, L.T. Recent progress in graphene-based electrodes for flexible batteries. *InfoMat* **2020**, *2*, 509–526. [CrossRef]
22. Gao, Y.; Zhao, N.; Li, J.; Liu, E.; He, C.; Shi, C. Hydrogen spillover storage on Ca-decorated graphene. *Int. J. Hydrogen Energy* **2012**, *37*, 11835–11841. [CrossRef]
23. Jian, N.; Xue, P.; Diao, D. Thermally induced atomic and electronic structure evolution in nanostructured carbon film by in situ TEM/EELS analysis. *Appl. Surf. Sci.* **2019**, *498*, 143831. [CrossRef]
24. Ye, Y.; Dai, L. Graphene-based Schottky junction solar cells. *J. Mater. Chem.* **2012**, *22*, 24224–24229. [CrossRef]
25. Yin, Z.; Zhu, J.; He, Q.; Cao, X.; Tan, C.; Chen, H.; Yan, Q.; Hua, Z. Graphene-Based Materials for Solar Cell Applications. *Adv. Energy Mater.* **2014**, *4*, 1300574. [CrossRef]
26. Lu, Q.; Zhang, L.L.; Cui, W.B.; Zhang, S.F.; Gong, W.J. Ab initio investigation of physical properties of the graphene/As-F hetero-bilayer. *Appl. Surf. Sci.* **2021**, *563*, 150339. [CrossRef]
27. Zhang, H.P.; Luo, X.G.; Lin, X.Y.; Lu, X.; Leng, Y. Density functional theory calculations of hydrogen adsorption on Ti-, Zn-, Zr-, Al-, and N-doped and intrinsic graphene sheets. *Int. J. Hydrogen Energy* **2013**, *38*, 14269–14275. [CrossRef]
28. Labroussea, J.; Belasfar, K.; Aziz, O.; Kenz, A.E.; Benyoussef, A. Two-dimensional GeC_3: A reversible, high-capacity hydrogen molecule storage material predicted by first-principles calculations. *Surf. Interfaces* **2022**, *31*, 101984. [CrossRef]
29. Sosa, A.N.; Cid, B.J.; Miranda, L. Light metal functionalized two-dimensional siligene for high capacity hydrogen storage: DFT study. *Int. J. Hydrogen Energy* **2021**, *46*, 29348–29360. [CrossRef]
30. Varunaa, R.; Ponniah, R. Potential hydrogen storage materials from metal decorated 2D-C_2N: An ab-initio study. *Phys. Chem. Chem. Phys.* **2019**, *21*, 25311–25322. [CrossRef]
31. Chan, K.T.; Neaton, J.B.; Cohen, M.L. First-principles study of metal adatom adsorption on graphene. *Phy. Rev. B* **2008**, *77*, 235430. [CrossRef]
32. Yang, S.L.; Wang, X.T.; Lei, G.; Xu, H.X.; Wang, Z.; Xiong, J.; Gu, H.S. A DFT study on the outstanding hydrogen storage performance of the Ti-decorated MoS_2 monolayer. *Surf. Interfaces* **2021**, *26*, 101329. [CrossRef]
33. Yamamoto, H.; Miyaoka, H.; Hino, S.; Nakanishi, H. Recyclable hydrogen storage system composed of ammonia and alkali metal hydride. *Int. J. Hydrogen Energy* **2009**, *34*, 9760–9764. [CrossRef]
34. Zuttel, A.; Borgschulte, A.; Orimo, S.I. Tetrahydroborates as new hydrogen storage materials. *Scr. Mater.* **2007**, *56*, 823–828. [CrossRef]
35. Cao, H.J.; Richter, T.M.M.; Pistidda, C.; Chaudhary, A.L. Ternary Amides Containing Transition Metals for Hydrogen Storage: A Case Study with Alkali Metal Amidozincates. *ChemSusChem* **2015**, *8*, 3777–3782. [CrossRef] [PubMed]
36. Seenithurai, S.; Pandyan, R.K.; Kumar, S.V.; Saranya, C.; Mahendran, M. Li-decorated double vacancy graphene for hydrogen storage application: A first principles study. *Int. J. Hydrogen Energy* **2014**, *39*, 11016. [CrossRef]
37. Chen, Y.D.; Yu, S.; Zhao, W.H. A potential material for hydrogen storage: A Li decorated graphitic-CN monolayer. *Phys. Chem. Chem. Phys.* **2018**, *20*, 13473. [CrossRef]
38. Liu, Z.Y.; Liu, S.; Er, S. Hydrogen storage properties of Li-decorated B_2S monolayers: A DFT study. *Int. J. Hydrogen Energy* **2019**, *44*, 16803–16810. [CrossRef]
39. Wang, Y.; Lü, J.; Zhu, L.; Ma, Y. Crystal Structure Prediction Via Particle-Swarm Optimization. *Phys. Rev. B* **2010**, *82*, 94116. [CrossRef]
40. Wang, Y.; Lv, J.; Zhu, L.; Ma, Y. CALYPSO: A Method for Crystal Structure Prediction. *Comput. Phys. Commun.* **2012**, *183*, 2063. [CrossRef]
41. Benzidi, H.; Lakhal, M.; Garara, M.; Mounkachi, O. Arsenene monolayer as an outstanding anode material for (Li/Na/Mg)-ion batteries: Density functional theory. *Phys. Chem. Chem. Phys.* **2019**, *21*, 19951. [CrossRef]
42. Ding, W.; Zhu, J.; Wang, Z.; Gao, Y.; Xiao, D.; Zhu, W. Prediction of Intrinsic Two-Dimensional Ferroelectrics inIn_2Se_3 and Other III_2-VI_3 van Der Waals Materials. *Nat. Commun.* **2017**, *8*, 14956. [CrossRef]
43. Wei, D.; Lin, Z.G.; Hu, C.W. Two-step fabrication of a porous γ-In_2Se_3 tetragonal photocatalyst for water splitting. *Chem. Comm.* **2013**, *49*, 9609–9611. [CrossRef] [PubMed]
44. Sim, Y.; Kim, J.; Seong, M.J. Simple synthesis of ultra-high quality In_2S_3 thin films on InAs substrates. *J. Alloys Compd.* **2016**, *685*, 518–522. [CrossRef]
45. Kresse, G.; Furthmüller, J. Efficiency of ab-initio total energy calculations for metals and semiconductors using a plane-wave basis set. *Comput. Mater. Sci.* **1996**, *6*, 15–50. [CrossRef]
46. Kresse, G.; Joubert, D. From ultrasoft pseudopotentials to the projector augmented-wave method. *Phys. Rev. B* **1999**, *59*, 1758. [CrossRef]
47. Perdew, J.P.; Burke, K.; Ernzerhof, M. Generalized Gradient Approximation Made Simple. *Phys. Rev. Lett.* **1996**, *77*, 3865. [CrossRef]
48. Grimme, S. Semiempirical GGA-type density functional constructed with a long-range dispersion correction. *J. Comput. Chem.* **2010**, *27*, 1787–1799. [CrossRef]
49. Ambrosetti, A.; Ferri, N.; Distasio, R.A. Wavelike charge density fluctuations and van der Waals interactions at the nanoscale. *Science* **2016**, *351*, 1171–1176. [CrossRef]

50. Monkhorst, H.J.; Pack, J.D. Special points for Brillouin-zone integrations. *Phys. Rev. B* **1976**, *13*, 5188. [CrossRef]
51. Nose, S. A unified formulation of the constant temperature molecular dynamics methods. *J. Chem. Phys.* **1984**, *81*, 511–519. [CrossRef]
52. Zhang, S.; Yan, Z.; Li, Y. Atomically Thin Arsenene and Antimonene: Semimetal-Semiconductor and Indirect-Direct Band-Gap Transitions. *Angew. Chem.* **2015**, *127*, 3112–3115. [CrossRef] [PubMed]
53. Rajput, K.; He, J.; Frauenheim, T.; Roy, D.R. Monolayer PC_3: A promising material for environmentally toxic nitrogen-containing multi gases. *J. Hazard* **2022**, *422*, 126761. [CrossRef] [PubMed]
54. Yang, W.; Xu, S.; Ma, K.; Wu, C.; Ding, X. Geometric structures, electronic characteristics, stabilities, catalytic activities, and descriptors of graphene-based single-atom catalysts. *Nano Mater. Sci.* **2020**, *2*, 120–131. [CrossRef]
55. Tavhare, P.; Titus, E.; Chaudhari, A. Boron substitution effect on adsorption of H_2 molecules on organometallic complexes. *Int. J. Hydrogen Energy* **2019**, *44*, 345–353. [CrossRef]